



1 **On the potential of Cluster Ion Counter (CIC) to observe local new particle formation,**  
2 **condensation sink and growth rate of newly formed particles**

3  
4 Markku Kulmala<sup>1,2,3</sup>, Santeri Tuovinen<sup>1</sup>, Sander Mirme<sup>4,5</sup>, Paap Koemets<sup>4,5</sup>, Lauri Ahonen<sup>1</sup>,  
5 Yongchun Liu<sup>2</sup>, Heikki Junninen<sup>4</sup>, Tuukka Petäjä<sup>1,2,3</sup> and Veli-Matti Kerminen<sup>1</sup>  
6

7  
8 <sup>1</sup> Institute for Atmospheric and Earth System Research (INAR)/Physics, University of  
9 Helsinki, Helsinki, 00014, Finland

10 <sup>2</sup> Aerosol and Haze Laboratory, Beijing Advanced Innovation Center for Soft Matter Science  
11 and Engineering, Beijing University of Chemical Technology, Beijing, 100089, China

12 <sup>3</sup> Joint International Research Laboratory of Atmospheric and Earth System Sciences, School  
13 of Atmospheric Sciences, Nanjing University, Nanjing, 210023, China

14 <sup>4</sup>Institute for Physics, University of Tartu, Tartu, 50090, Estonia

15 <sup>5</sup>Airel Ltd., Observatooriumi 5, 61602 Tõravere, Estonia  
16

17 Keywords: atmospheric ions, ion measurements, cluster ions, intermediate ions,  
18 instrumentation, new particle formation, condensation sink  
19

20  
21 *Correspondence to:* Markku Kulmala (markku.kulmala@helsinki.fi)  
22

23 **Abstract**  
24

25 Cluster Ion Counter (CIC) is a simple 3-channel instrument designed to observe ions in the  
26 diameter range from 1.0 to 5 nm. With the three channels, we can observe concentrations of  
27 both ion clusters (sub-2 nm ions) and intermediate ions. Furthermore, as derived here, we can  
28 estimate condensation sink, intensity of local new particle formation, growth rate of newly  
29 formed particles from 2 nm to 3 nm, and formation rate of 2 nm ions. We compared CIC  
30 measurements with those of a multichannel ion spectrometer, the Neutral cluster and Air Ion  
31 Spectrometer (NAIS), and found that the concentrations agreed well between the two  
32 instruments, with the correlation coefficients of 0.89 and 0.86 for sub-2 nm and 2.0–2.3 nm  
33 ions, respectively. According to the observations made in Hyytiälä, Finland and Beijing,  
34 China, the ion source rate was estimated to be about 2–4 ion pairs cm<sup>-3</sup> s<sup>-1</sup>.  
35

36 **1. Introduction**  
37

38 New particle formation (NPF) is the dominant source of the number concentration of aerosol  
39 particles in the global atmosphere (Gordon et al., 2017), thereby having potentially large  
40 influences on global climate (e.g. Boucher et al., 2013) and regional air quality (e.g. Guo et  
41 al., 2014; Kulmala et al., 2022). During the past 2-3 decades, atmospheric NPF has been  
42 characterized in terms of the particle formation and growth rates at a vast variety of sites in  
43 different atmospheric environments (Wang et al., 2017; Kerminen et al., 2018; Nieminen et  
44 al., 2018; Chu et al., 2019; Bousiotis et al., 2021). Such characteristics describe mainly  
45 regional NPF, i.e. NPF averaged over relatively large spatial scales of at least tens of km.  
46 Much less information is available about local NPF, or about the small-scale variability of  
47 regional NPF. Such information would be important in identifying hot spot areas for  
48 atmospheric NPF, or estimating the relative importance of various local sources to regional  
49 NPF.  
50



51 Atmospheric cluster ion (diameters below 2 nm) measurements can provide insight into ion  
52 source processes, such as the ion production rate associated with different atmospheric  
53 ionization pathways, as well as ion loss processes, such as ion-ion recombination or  
54 scavenging of ions by a pre-existing atmospheric aerosol population (e.g. Hirsikko et al.,  
55 2011; Kontkanen et al., 2013). Observations of intermediate ions (diameters between 2 and 7  
56 nm) can be used to get information about atmospheric NPF (e.g. Tammet et al., 2014),  
57 whereas small intermediate ions (approx. 2–2.3 nm) can be used to detect "local" NPF, i.e.  
58 NPF taking place within a close proximity of a measurement site (Tuovinen et al., 2024).

59  
60 Intermediate ions are sensitive to both occurrence and intensity of atmospheric NPF (e.g.  
61 Horrak et al., 1998; Tammet et al., 2014, Leino et al., 2016). Recently, Kulmala et al. (2024)  
62 and Tuovinen et al. (2024) found that the smallest sizes of intermediate ions describe  
63 relatively well the local production of new aerosol particles. These results were obtained  
64 using a Neutral Cluster and Air Ion Spectrometer (NAIS; Mirme and Mirme, 2013). The  
65 NAIS is, however, a sophisticated instrument that provides information not necessarily  
66 needed when investigating local NPF.

67  
68 In this study, we will analyse data obtained using a Cluster Ion Counter (CIC; Mirme et al.,  
69 2024), a recently developed and simple 3-channel instrument, and will investigate how this  
70 instrument can be utilized to determine several variables important to NPF and small ion  
71 dynamics. Our main objectives are to derive simple equations for characterizing ion  
72 dynamics related to local NPF, and to find out whether the CIC is sensitive and reliable  
73 enough for such purposes. In order to reach these objectives, we will first derive equations  
74 that can be used to estimate condensation sink (CS), intensity of local new particle formation  
75 (actually local intermediate ion formation, LIIF), growth rate of newly formed particles and  
76 formation rate of 2 nm ions based on CIC measurements. Next, we will compare ion  
77 concentrations between the CIC and NAIS, as measured at the SMEAR II station in Hyytiälä,  
78 Finland. Finally, we will demonstrate how to apply CIC measurements in practice for  
79 obtaining information about local NPF and related quantities, including the condensation  
80 sink.

## 81 82 **2. Material and Methods**

### 83 84 **2.1 Cluster Ion Counter (CIC)**

85  
86 The Cluster Ion Counter (CIC) is designed to be a simple and robust instrument for  
87 measuring total concentrations of small ions, and for obtaining some additional information  
88 about ion size distributions. The CIC has a low size resolution, with only three separate  
89 electrometers (Mirme et al., 2024). The mobility ranges of the three collecting electrodes of  
90 the original CIC were chosen to allow the estimation of average cluster ion mobility.  
91 However, the analyzer of the device can easily be modified to focus on other aspects of the  
92 mobility distribution.

93  
94 A modified analyzer for the CIC was developed to estimate the concentration of intermediate  
95 ions roughly between 2 and 2.3 nm. Due to the relatively simple construction of the CIC, and  
96 specifically the absence of a separate sheath air flow layer in the mobility analyzer, the  
97 detection efficiency curves of the individual electrodes of the CIC are relatively wide and  
98 extend far towards larger particles (Figure 1). A higher size resolution can be achieved by  
99 looking at the difference of a signal between two separate channels. In the modified CIC, the  
100 signal from the first electrometer can be used to estimate the cluster ion concentrations. By



101 subtracting the signal of the third channel from the signal of the second channel, the  
102 concentration of intermediate ions roughly between 2 and 2.3 nm can be estimated. The third  
103 channel can be utilized for ions from 2.3 to 5 nm.

104

## 105 2.2 Conceptual model

106

107 The time evolution of sub-2 nm ion concentration,  $I$ , can be written as

108

$$109 \frac{dI}{dt} = Q - \alpha I^2 - \text{CoagS}_I \times I, \quad (1)$$

110

111 where  $Q$  is the ion source rate,  $\alpha$  ( $\approx 1.6 \times 10^{-6} \text{ cm}^{-3} \text{ s}^{-1}$ ; Franchin et al., 2015) is the ion-ion  
112 recombination rate, and  $\text{CoagS}_I$  is the coagulation sink of the sub-2 nm ions onto pre-existing  
113 aerosol particles. In a steady state, we may approximate the left-hand side of eq. 1 equal to  
114 zero, from which we obtain:

115

$$116 \text{CoagS}_I = Q/I - \alpha I. \quad (2)$$

117

118 The coagulation sink of particles of diameter  $d_p$  can be connected with the condensation sink  
119 (CS) of sulphuric acid monomers via (see Lehtinen et al., 2007)

120

$$121 \text{CS} \approx \text{CoagS}(d_p) (d_p/0.7 \text{ nm})^m, \quad (3)$$

122

123 where the exponent  $m$  depends on the shape of the pre-existing particle number size  
124 distribution, and the diameter of a sulphuric acid monomer is estimated to be 0.7 nm. By  
125 combining eqs. 2 and 3 we then obtain:

126

$$127 \text{CS} \approx \text{CoagS}(d_p = d_{p,1}) / \text{CoagS}_I (d_p/0.7 \text{ nm})^m (Q/I - \alpha I), \quad (4)$$

128

129 where  $d_{p,1}$  refers to the median diameter of the sub-2 nm ions. In order to simplify eq. 4, we  
130 will make three further approximations: 1)  $d_{p,1}$  is equal to 1.2 nm for negative cluster ions  
131 observed with CIC, and 1.0 nm for negative cluster ions measured with NAIS, 2) the  
132 exponent  $m$  is equal to 1.6 (see Lehtinen et al., 2007), and 3) the ratio  $\text{CoagS}(d_p = d_{p,1}) /$   
133  $\text{CoagS}_I$  is equal to 0.5 (Leppä et al., 2011; Mahfourz and Donahue, 2021). By combining  
134 these approximations, we finally obtain:

135

$$136 \text{CS} \approx 1.2 (Q/I - \alpha I). \quad (5a)$$

137

$$138 \text{CS} \approx 0.9 (Q/I - \alpha I). \quad (5b)$$

139

140 If  $I$  is measured with the CIC (NAIS), we can utilize eq. 5a (5b).

141

142 Similar to eq. 1, the time evolution of the concentration of the smallest (2–2.3 nm)  
143 intermediate ions,  $N$ , can be written as

144

$$145 \frac{dN}{dt} = J_2 - \text{CoagS}_N \times N - J_{\text{out}}, \quad (6)$$

146

147 where  $J_2$  is the formation rate of 2 nm ions,  $\text{CoagS}_N$  is the coagulation sink of the 2.0–2.3 nm  
148 ions onto the pre-existing aerosol population, and  $J_{\text{out}}$  is the rate at which these ions grow out  
149 of the 2.0–2.3 nm size range.  $\text{CoagS}_N$  and  $J_{\text{out}}$  can be approximated as:



150  
151  $\text{CoagS}_N \approx \text{CoagS}_1 \times (1.2 \text{ nm} / 2.1 \text{ nm})^{1.6} \approx 0.4 \text{ CoagS}_1 \approx 0.4 (Q/I - aI),$  (7)

152  
153  $J_{\text{out}} \approx \text{GR}_{2.3 \text{ nm}} \times N/\Delta d,$  (8)

154  
155 where  $\text{GR}_{2.3 \text{ nm}}$  is the growth rate of 2.3 nm ions and  $\Delta d (=0.3 \text{ nm})$  is the width of the  
156 intermediate ion channel of the CIC. Assuming a steady state ( $dN/dt = 0$ ) and using Eqs. 2, 7  
157 and 8, we then obtain:

158  
159  $J_2 = 0.4 (Q/I - aI) \times N + \text{GR}_{2.3 \text{ nm}} \times N/\Delta d + aIN.$  (9)

160  
161 The last term in Eq. 9 accounts for the loss rate of 2.0-2.3 nm ions due to their recombination  
162 with sub-2 nm ions.

163  
164 Particle (or ion) growth rates can be determined from the following equation:

165  
166  $\text{GR} = \frac{\Delta d_i}{\Delta t},$  (10)

167  
168 where  $\Delta d_i$  is the change of the diameter of ions over the time interval  $\Delta t$  as the ions grow in  
169 size. In section 3.2 we will demonstrate how the CIC measurement can be used for  
170 determining growth rates.

## 171 172 **2.3. Observations**

173  
174 The CIC and NAIS were compared with each other at the SMEAR II station in Hyytiälä (Hari  
175 and Kulmala, 2005) during 16 January–01 April, 2024; however, NAIS data were missing  
176 from the period 16–17 March. The NAIS (Neutral Cluster and Air Ion Spectrometer) is a  
177 multichannel instrument to measure atmospheric ions from 0.8 to 42 nm and total particle  
178 concentrations from 2.5 to 42 nm (Mirme and Mirme, 2013). Furthermore, the conceptual  
179 model was used to analyse the data from both SMEAR II and AHL/BUCT station in Beijing,  
180 China (Liu et al., 2020). To produce Figure 6, 10%, 25%, 50%, 75%, and 90% small ion  
181 concentrations and CS values were used. The ion concentration values were also used in  
182 Figures 8 and 9. These data were taken from a different, longer time span than the data used  
183 for the CIC and NAIS comparison. For Hyytiälä, the data cover most of the time between the  
184 beginning of 2016 and end of 2020. For Beijing, ion concentrations were determined over the  
185 period 13 January 2018 to 01 April 2020, whereas the CS data cover the period 20  
186 February 2018 to 31 March 2019. The particle number size distributions to derive the CS data  
187 were measured by a twin DMPS (Differential Mobility Particle Sizer; Aalto et al., 2001) in  
188 Hyytiälä and in Beijing by a particle size distribution (PSD) system (Liu et al., 2016). See  
189 Zhou et al. (2020) for more details on the measurements in Beijing.

## 190 191 192 **3. Results and Discussion**

### 193 194 **3.1 Instrument comparison**

195  
196 In order to find out how reliably the CIC is able to observe ion concentrations, we compared  
197 it with the NAIS at the SMEAR II station in Hyytiälä, Finland. Tables 1 and 2 summarize the  
198 statistics of the ion concentrations measured by these two instruments for different size  
199 fractions. We can see that the total concentration of sub-2 nm negative ions measured by the



200 NAIS is significantly higher than those measured by the CIC (channel 1), the median  
201 concentrations being equal to 530 and 210  $\text{cm}^{-3}$ , respectively. However, excluding the  
202 smallest ions measured by the NAIS, i.e. considering only the 1–2 nm size range, the median  
203 concentration drops down to 180  $\text{cm}^{-3}$ . This is slightly below the median sub-2 nm  
204 concentration measured by the CIC, but only about one third of the median total sub-2 nm ion  
205 concentration measured by the NAIS.

206  
207 A detailed comparison between the two instruments is in Figure 2 for small ( $<2$  nm) ions, and  
208 in Figure 3 for the smallest size class of intermediate ions (2.0–2.3 nm). We can see that  
209 while the CIC shows somewhat larger small ion (1–2 nm) and lower 2.0–2.3 nm ion  
210 concentrations compared with the NAIS, the overall agreement between these two  
211 instruments is very good with the correlation coefficients of 0.85 and 0.86 for small ions and  
212 2.0–2.3 nm ions, respectively.

213  
214 Figure 4 presents the time series of ion concentrations measured by the CIC and NAIS over  
215 the whole two and half-month period, while Figure 5 presents the diurnal pattern of ions  
216 concentrations on a selected day (10<sup>th</sup> of March, 2024). Both size classes (sub-2 nm and 2.0–  
217 2.3 nm) agree pretty well between the two instruments, the correlation coefficient being  
218 around 0.9 on the selected day for both sub-2 nm ions and 2–2.3 nm ions. The peaks in 2.0–  
219 2.3 nm ion concentration are captured consistently by both instruments, and the concentration  
220 values of such peaks agree very well between the two instruments. Also the small ion  
221 concentrations agree well in terms of their peak values.

### 222 223 **3.2 Application of CIC measurement in investigating condensation sink and local NPF**

224  
225 Figure 6 illustrates how the estimated condensation sink (CS) based on Eq. 5 behaves as a  
226 function of small ion concentrations,  $I$ , for different ion production rates. In the same plot, we  
227 have included the observed variability of CS and  $I$  in both Hyytiälä and Beijing. We can see  
228 that measured and theoretically calculated values of CS agree with each other the best when  
229 median ion production rates are between about 2 and 4 ion pairs  $\text{cm}^{-3} \text{s}^{-1}$  in both Hyytiälä and  
230 Beijing.

231  
232 The CIC has a higher detection efficiency for small ions than the NAIS due to a shorter inlet  
233 tract, and consequently, lower inlet losses. However, in case of both instruments, the  
234 detection efficiency for sub-2 nm ions is very strongly dependent on a particle size. The  
235 NAIS measures the size distribution of ions, and the data inversion algorithm uses that  
236 information to correct for the size-dependent detection efficiency. The CIC has limited  
237 information about the size distribution of detected ions, making it more difficult to correct for  
238 the detection efficiency. Using inverted ion size distribution data from the NAIS and  
239 uncorrected ion concentration data from the CIC (Tables 1 and 2), we estimated how the  
240 concentrations measured using the CIC and NAIS will influence the estimated values of CS.  
241 By using eq. 5 and by assuming the median sub-2 nm ion concentrations measured by these  
242 two instruments (Tables 1 and 2), we may calculate that the values of CS measured using the  
243 NAIS are 0.237, 256 and 0.266 times those measured using the CIC for  $Q$  equal to 2, 3 and 4,  
244 respectively. Therefore, if we use the CIC for estimating CS via eq. 5a, the real CS (using  
245 NAIS and equation 5b) is about 0.25 times the one observed by CIC.

246  
247 In order to illustrate how the CIC can be used to determine the growth rate, we selected one  
248 measurement day (Figure 7). We used the appearance time method (e.g. Lehtipalo et al.,  
249 2014) from channel 3 and the difference between channels 2 and 3. The difference in



250 channels gives the concentration in size range of 2.0–2.3 nm. The peak in the collection  
251 efficiency curve of channel 3 is approximately 2.9 nm (see Figure 1). So comparing the  
252 appearance time in those channels we can determine the growth rate from 2.1 to 2.9 nm to be  
253 about 1.0 nm/h. This value can be considered a very realistic one, as the earlier long-term  
254 measurements at the same site indicate typical growth rates between about 1 and 2 nm/h for  
255 sub-3 nm ions (Hirsikko et al., 2005; Manninen et al., 2010). We should note, however, that it  
256 is not possible to determine growth rates for all measurement days using the procedure  
257 illustrated in Figure 7. This is because even if an increase in ion concentrations was observed,  
258 the signal might be too noisy, making the determination of appearance times too unreliable.  
259 In addition, not all days exhibited a clear delay between the two appearance times, making  
260 the determination of growth rate impossible.

261  
262 Using eq. 9, we can estimate the formation rate of 2 nm ions,  $J_2$ . Figures 8 and 9 show these  
263 formation rates for Hyytiälä and Beijing, respectively. This formation rate can be given as a  
264 function of the measured number concentrations of 2.0–2.3 nm intermediate ions, in addition  
265 to which  $J_2$  depends on the growth rate, ion source rate, and ion loss rate.  $J_2$  also depends on  
266 the concentration of sub-2 nm ions, which is determined by the ion loss rate and ion source  
267 rate (Eq. 1). The most probable values are 1–2 nm/h for the growth rate in Hyytiälä (Figure 7,  
268 Hirsikko et al., 2005; Manninen et al., 2010), 1–3 nm/h for the growth rate in Beijing (Deng  
269 et al., 2020), and 2–3  $\text{cm}^{-3} \text{s}^{-1}$  for the ion source rate (Figure 6). However, also higher values  
270 are given for comparison. Manninen et al. (2010) calculated a median value of 0.06  $\text{cm}^{-3} \text{s}^{-1}$   
271 for  $J_2$  based on long-term measurements in Hyytiälä, which is at the higher end of values  
272 estimated in Figure 8. Compared with Hyytiälä, we estimate a factor of 2–4 larger values of  
273  $J_2$  for Beijing. In both places, the total formation rate of 2 nm particles is considerably larger  
274 than the formation rate of 2 nm ions, being of the order of one magnitude in Hyytiälä  
275 (Manninen et al., 2010, Kulmala et al., 2013) and even larger in Beijing (Deng et al., 2020).

276  
277 Figure 10 shows the estimated time evolution of the condensation sink and 2-nm ion  
278 formation rate during one day. The value of CS varies only little, less than a factor of 1.5,  
279 whereas the ion formation rate varies by more than two orders of magnitude during the day.  
280 We can clearly see that when CS is at its lowest at around midday, the ion formation rate is at  
281 its highest.

282

283

#### 284 4. Conclusions and summary

285

286 The recent progress of finding local NPF (e.g. Kulmala et al., 2024; Tuovinen et al., 2024)  
287 has opened a question: are we able to utilise a simple ion counter to find out LIIF in a proper  
288 way. According to our results presented above, the answer is: yes.

289

290 We have developed a somewhat modified version of the CIC to measure sub-2 nm ion and  
291 2.0–2.3 nm ion concentrations as accurately as possible (Mirme et al., 2024). From the latter  
292 quantity we can estimate LIIF (Kulmala et al., 2024; Tuovinen et al., 2024), and from the  
293 former quantity we get information on the dynamics of small ions, including an estimate of  
294 ion sinks and via equations (2) and (5) also condensation sink. Furthermore, the CIC makes it  
295 possible to estimate the growth rate from about 2 nm to 3 nm and, with this information, the  
296 formation rate of 2-nm ions. While we have focused on negative ions in this paper, the same  
297 is also valid for positive ions. LIIF is more sensitive to negative ions (Tuovinen et al., 2024),  
298 and thus negative ions were investigated.

299



300 The comparison of the estimated condensation sinks with the observed ones in Hyytiälä and  
301 Beijing shows that the CIC, together with the simple theoretical framework, is able to give  
302 relatively accurate estimates on the condensation sink, ion sinks and ion formation rates. We  
303 also compared the CIC with the NAIS in Hyytiälä, which demonstrates that the measured ion  
304 concentrations agree pretty well. Therefore, we can conclude that the CIC is an effective  
305 instrument to observe LIIF and CS. However, if we want to investigate aerosol formation and  
306 growth rates for the nucleation mode (3–25 nm), as is usually the case in investigating  
307 regional NPF, NAIS measurements are needed.

308

### 309 **Author contribution**

310

311 Markku Kulmala had the original idea after discussions with Heikki Junninen. SM and PK  
312 developed the CIC. LA performed CIC and NAIS comparison in Hyytiälä. ST and MK  
313 analyzed the data. VMK and MK derived the used equations. YL lead the observations in  
314 Beijing and TP in Hyytiälä. HJ, VMK, TP and ST contributed to developing the idea further.  
315 MK, VMK and ST wrote the first version of the paper. All coauthors contributed the final  
316 version of the paper.

317

### 318 **Competing interests**

319

320 Markku Kulmala is a member of the editorial board of Aerosol Research. The authors have  
321 no other competing interests to declare.

322

### 323 **Acknowledgements**

324 We acknowledge the following projects: ACCC Flagship funded by the Academy of Finland  
325 grant number 337549 (UH) and 337552 (FMI), Academy professorship funded by the Academy  
326 of Finland (grant no. 302958), Academy of Finland projects no. 1325656, 311932, 334792,  
327 316114, 325647, 325681, 347782, “Quantifying carbon sink, CarbonSink+ and their  
328 interaction with air quality” INAR project funded by Jane and Aatos Erkkö Foundation,  
329 “Gigacity” project funded by Wihuri foundation, European Research Council (ERC) project  
330 ATM-GTP Contract No. 742206, European Union via Non-CO<sub>2</sub> Forcers and their Climate,  
331 Weather, Air Quality and Health Impacts (FOCI), and Estonian Research Council project  
332 PRG71. University of Helsinki support via ACTRIS-HY is acknowledged. University of  
333 Helsinki Doctoral Programme in Atmospheric Sciences and the High-End Foreign Expert  
334 Recruitment Program of China (G2023106004L) is acknowledged. Support of the technical  
335 and scientific staff in Hyytiälä SMEAR II station and AHL/BUCT station in Beijing are  
336 acknowledged.

337

### 338 **References**

339

Aalto, P., Hämeri, K., Becker, E., Weber, R., Salm, J., Mäkelä, J. M., Hoell, C., O’ Dowd, C.  
D., Hansson, H.-C., Väkevä, M., Koponen, I. K., Buzorius, G., and Kulmala, M.: Physical  
characterization of aerosol particles during nucleation events, *Tellus B*, 53, 344–358,  
doi:10.1034/j.1600-0889.2001.530403.x, 2001.



Boucher, O., Randall, D., Artaxo, P., Bretherton, C., Feingold, G., Forster, P., Kerminen, V.-M., Kondo, Y., Liao, H., Lohmann, U., Rasch, P., Satheesh, S., Sherwood, S., Stevens, B., and Zhan, X.: Clouds and Aerosols, in: *Climate Change 2013: The Physical Science Basis. Contribution of Working Group I to the Fifth Assessment Report of the Intergovernmental Panel on Climate Change*, edited by: Stocker, T., Qin, D., Plattner, G., Tignor, M., Allen, S., Boschung, J., Nauels, A., Xia, Y., Bex, V., and Midgley, P., Cambridge University Press, Cambridge, United Kingdom and New York, NY, USA, 2013.

Bousiotis, D., Pope, F. D., Beddows, D. C. S., Dall'Osto, M., Massling, A., Nøjgaard, J. K., Nordstrøm, C., Niemi, J. V., Portin, H., Petäjä, T., Perez, N., Alastuey, A., Querol, X., Kouvarakis, G., Mihalopoulos, N., Vratolis, S., Eleftheriadis, K., Wiedensohler, A., Weinhold, K., Merkel, M., Tuch, T., and Harrison, R. M.: A phenomenology of new particle formation (NPF) at 13 European sites, *Atmos. Chem. Phys.*, 21, 11905–11925, <https://doi.org/10.5194/acp-21-11905-2021>, 2021.

Chu, B., Kerminen, V.-M., Bianchi, F., Yan, C., Petäjä, T., and Kulmala, M.: Atmospheric new particle formation in China, *Atmos. Chem. Phys.*, 19, 115–138, <https://doi.org/10.5194/acp-19-115-2019>, 2019.

Deng, C., Fu, Y., Dada, L., Yan, C., Cai, R., Yang, D., Zhou, Y., Yin, R., Lu, Y., Li, X., Qiao, X., Fan, X., Nie, W., Kontkanen, J., Kangasluoma, J., Chu, B., Ding, A., Kerminen, V.-M., Paasonen, P., Worsnop, D. R., Bianchi, F., Liu, Y., Zheng, J., Wang, L., Kulmala, M., and Jiang, J.: Seasonal characteristics of new particle formation and growth in Urban Beijing, *Environ. Sci. Technol.*, 54, 8547–8557, 2020.

Franchin, A., Ehrhart, S., Leppä, J., Nieminen, T., Gagne, S., Schobesberger, S., Wimmer, D., Duplissy, J., Riccobono, F., Dunne, E. M., Rondo, L., Downard, A., Bianchi, F., Kupc, A., Tsagkogeorgas, G., Lehtipalo, K., Manninen, H. E., Almeida, J., Amorim, A., Wagner, P. E., Hansel, A., Kirkby, J., Kurten, A., Donahue, N. M., Makhmutov, V., Mathot, S., Metzger, A., Petäjä, T., Schnitzhofer, R., Sipilä, M., Stozhkov, Y., Tome, A., Kerminen, V.-M., Carslaw, K., Curtius, J., Baltensperger, U., and Kulmala, M.: Experimental investigation of ion-ion recombination under atmospheric conditions, *Atmos. Chem. Phys.*, 15, 7203–7216, 2015.

Gordon, H., Kirkby, J., Baltensperger, U., Bianchi, F., Breitenlechner, M., Curtius, J., Dias, A., Dommen, J., Donahue, N. M., Dunne, E. M., Duplissy, J., Ehrhart, S., Flagan, R. C., Frege, C., Fuchs, C., Hansel, A., Hoyle, C. R., Kulmala, M., Kürten, A., Lehtipalo, K., Makhmutov, V., Molteni, U., Rissanen, M. P., Stozhov, Y., Tröstl, J., Tsakogeorgas, G., Wagner, R., Williamson, C., Wimmer, D., Winkler, P. M., Yan, C., and Carslaw, K. S.: Causes and importance of new particle formation in the present-day and preindustrial atmospheres. *J. Geophys. Res. Atmos.*, 122, 8739–8760, <https://doi.org/10.1002/2017JD026844>, 2017.

Guo, S., Hu, M., Zamora, M. L., Peng, J., Shang, D., Zheng, J., Du, Z., Wu, Z., Shao, M., Zeng, L., Molina, M. J., and Zhang, R.: Elucidating severe urban haze formation in China, *Proc. Natl. Acad. Sci. U.S.A.*, 111, 17373, <https://doi.org/10.1073/pnas.1419604111>, 2014.

Hari, P. and Kulmala, M.: Station for measuring Ecosystem-Atmosphere relations (SMEAR II), *Boreal Environment Research*, 10, 2005.

Hirsikko, A., Laakso, L., Hörrak, U., Aalto, P. P., Kerminen, V.-M., and Kulmala, M.: Annual and size dependent variation of growth rates and ion concentrations in boreal forest, *Boreal Env. Res.*, 10, 357–369, 2005.



Hirsikko, A., Nieminen, T., Gagne, S., Lehtipalo, K., Manninen, H. E., Ehn, M., Horrak, U., Kerminen, V.-M., Laakso, L., McMurry, P. H., Mirme, A., Mirme, S., Petäjä, T., Tammet, H., Vakkari, V., Vana, M., and Kulmala, M.: Atmospheric ions and nucleation: a review of observations, *Atmos. Chem. Phys.*, 11, 767–798, 2011.

Horrak, U., Salm, J., and Tammet, H.: Bursts of intermediate ions in atmospheric air, *J. Geophys. Res.-Atmos.*, 103(D12), 13909–13915, 1998.

Kerminen, V.-M., Chen, X., Vakkari, V., Petäjä, T., Kulmala, M., and Bianchi, F.: Atmospheric new particle formation and growth: review of field observations, *Environ. Res. Lett.*, 13, 103003, DOI 10.1088/1748-9326/aadf3c, 2018.

Kontkanen, J., Lehtinen, K. E. J., Nieminen, T., Manninen, H. E., Lehtipalo, K., Kerminen, V.-M., and Kulmala, M.: Estimating the contribution of ion-ion recombination to sub-2 nm cluster concentrations from atmospheric measurements, *Atmos. Chem. Phys.*, 13, 11391–11401, 2013.

Kulmala, M., Kontkanen, J., Junninen, H., Lehtipalo, K., Manninen, H. E., Nieminen, T., Petäjä, T., Sipilä, M., Schobesberger, S., Rantala, P., Franchin, A., Jokinen, T., Järvinen, E., Äijälä, M., Kangasluoma, J., Hakala, J., Aalto, P. P., Paasonen, P., Mikkilä, J., Vanhanen, J., Aalto, J., Hakola, H., Makkonen, U., Ruuskanen, T., Mauldin, R. L., Duplissy, J., Vehkamäki, H., Bäck, J., Kortelainen, A., Riipinen, I., Kurtén, T., Johnston, M. V., Smith, J. N., Ehn, M., Mentel, T. F., Lehtinen, K. E. J., Laaksonen, A., Kerminen, V.-M., and Worsnop, D. R.: Direct observations of atmospheric aerosol nucleation, *Science*, 339, 943–946, <https://doi.org/10.1126/science.1227385>, 2013.

Kulmala, M., Cai, R., Stolzenburg, D., Zhou, Y., Dada, L., Guo, Y., Yan, C., Petäjä, T., Jiang, J., and Kerminen, V.-M.: The contribution of new particle formation and subsequent growth to haze formation, *Environ. Sci.: Atmos.*, 2, 352–361, 2022

Kulmala, M., Ke, P., Lintunen, A., Peräkylä, O., Lohtander, A., Tuovinen, S., Lampilahti, J., Kolari, P., Schiestl-Aalto, P., Kokkonen, T., Nieminen, T., Dada, L., Ylivinkka, I., Petäjä, T., Bäck, J., Lohila, A., Heimsch, L., Ezhova, E., and Kerminen, V.-M.: A novel concept for assessing the potential of different boreal ecosystems to mitigate climate change (CarbonSink+ Potential). *Boreal Env. Res.*, 29, 1–16, 2024.

Lehtinen, K. E. J., Dal Maso, M., Kulmala, M., and Kerminen V.-M.: Estimating nucleation rates from apparent particle formation rates and vice-versa: Revised formulation of the Kerminen-Kulmala equation, *J. Aerosol Sci.*, 38, 988–994, 2007.

Lehtipalo, K., Leppä, J., Kontkanen, J., Kangasluoma, J., Franchin, A., Wimmer, D., Schobesberger, S., Junninen, H., Petäjä, T., Sipilä, M., Mikkilä, J., Vanhanen, J., Worsnop, D. R., and Kulmala, M.: Methods for determining particle size distribution and growth rates between 1 and 3 nm using the Particle Size Magnifier, *Boreal Environ. Res.*, 19, 215–236, 2014.

Leino, K., Nieminen, T., Manninen, H. E., Petäjä, T., Kerminen, V.-M., and Kulmala, M.: Intermediate ions as a strong indicator of new particle formation bursts in boreal forest, *Boreal Env. Res.*, 21, 274–286, 2016.



Leppä, J., Anttila, T., Kerminen, V.-M., Kulmala, M., and Lehtinen, K. E. J.: Atmospheric new particle formation: real and apparent growth of neutral and charged particles, *Atmos. Chem. Phys.*, 11, 4939-4955, 2011.

Liu, J. Q., Jiang, J. K., Zhang, Q., Deng, J. G., and Hao, J. M.: A spectrometer for measuring particle size distributions in the range of 3 nm to 10  $\mu\text{m}$ , *Front. Env. Sci. Eng.*, 10, 63–72, <https://doi.org/10.1007/s11783-014-0754-x>, 2016.

Liu Y., Yan C., Feng Z., Zheng F., Fan X., Zhng Y., Li C., Zhou Y, Lin Z., Guo Y., Zhang Y., Ma L., Zhou W., Liu Z., Dada L., Dällenback K., Kontkanen J., Cai R., Chan T., Chu B., Du W., Yao L., Wang Y., Cai J., Kangasluoma J., Kokkonen T., Kujansuu J., Rusanen A., Deng C., Fu Y., Yin R., Li X., Lu Y., Liu Y., Lian C., Yang D., Wang W., Ge M., Wang Y., Worsnop D. R., Junninen H., He H. Kerminen V.-M., Zheng J., Wang L., Jiang J., Petäjä T., Bianchi F. and Kulmala M. (2020) Continuous and comprehensive atmospheric observations in Beijing: a station to understand the complex urban atmospheric environment. *Big Earth Data* 4, 295-321.

Mahfouz, N. G. A. and Donahue, N. M.: Technical note: The enhancement limit of coagulation scavenging of small charged particles. *Atmos. Chem. Phys.*, 21, 3827-3832, 2021.

Manninen, H. E., Nieminen, T., Asmi, E., Gagne, S., Häkkinen, S., Lehtipalo, K., Aalto, P., Vana, M., Mirme, A., Mirme, S., Hörrak, U., Plass-Dülmer, C., Stange, G., Kiss, G., Hoffer, A., Töro, N., Moerman, M., Henzing, B., de Leeuw, G., Brinkenberg, M., Kouvarakis, G. N., Bougiatioti, A., Mihalopoulos, N., O'Dowd, C. D., Ceburnis, D., Arneth, A., Svenningsson, B., Swietlicki, E., Tarozzi, L., Decesari, S., Facchini, M. C., Birmili, W., Sonntag, A., Wiedensohler, A., Boulon, J., Sellegri, K., Laj, P., Gysel, M., Bukowiecki, N., Weingartner, E., Wehrle, G., Laaksonen, A., Hamed, A., Joutsensaari, J., Petäjä, T., Kerminen, V.-M., and Kulmala, M.: EUCAARI ion spectrometer measurements at 12 European sites – analysis of new particle formation events, *Atmos. Chem. Phys.*, 10, 7907-7927, 2020.

Mirme, S. and Mirme, A.: The mathematical principles and design of the NAIS – a spectrometer for the measurement of cluster ion and nanometer aerosol size distributions, *Atmos. Meas. Tech.*, 6, 1061–1071, doi:10.5194/amt-6-1061-2013, 2013.

Mirme, S., Manninen, H.E., Koemets, Balbaaki, R., Rörup B., Wu, Y., Ehrhart, S., Weber, S.K., Pfeifer, J., Kangasluoma, J., Kulmala, M., and Kirkby, J. Design and evaluation of Cluster Ion Counter (CIC) with low noise and fast time response, to be submitted to *Atmos. Meas. Tech.*, 2024

Nieminen, T., Kerminen, V.-M., Petäjä, T., Aalto, P. P., Arshinov, M., Asmi, E., Baltensperger, U., Beddows, D. C. S., Beukes, J. P., Collins, D., Ding, A., Harrison, R. M., Henzing, B., Hooda, R., Hu, M., Hörrak, U., Kivekäs, N., Komsaare, K., Krejci, R., Kristensson, A., Laakso, L., Laaksonen, A., Leaitch, W. R., Lihavainen, H., Mihalopoulos, N., Németh, Z., Nie, W., O'Dowd, C., Salma, I., Sellegri, K., Svenningsson, B., Swietlicki, E., Tunved, P., Ulevicius, V., Vakkari, V., Vana, M., Wiedensohler, A., Wu, Z., Virtanen, A., and Kulmala, M.: Global analysis of continental boundary layer new particle formation based on long-term measurements, *Atmos. Chem. Phys.*, 18, 14737–14756, <https://doi.org/10.5194/acp-18-14737-2018>, 2018.



Tammet, H, Komsaare, K., and Horrak, U.: Intermediate ions in the atmosphere, *Atmos. Res.*, 135-136, 263-273, <https://doi.org/10.1016/j.atmosres.2012.09.009>, 2014.

Tuovinen, S., Lampilahti, J., Kerminen, V.-M., and Kulmala, M.: Intermediate ions as indicator for local new particle formation, *Aerosol Research Discuss.* [preprint], in review, 2024.

Wang, Z., Wu, Z., Yue, D., Shang, D., Guo, S., Sun, J., Ding, A., Wang, L., Jiang, J., Guo, H., Gao, J., Cheung, H. C., Morawska, L., Keywood, M., and Hu, M.: New particle formation in China: Current knowledge and further directions, *Sci. Total Environ.*, 577, 258-266, 2017.

Zhou, Y., Dada, L., Liu, Y., Fu, Y., Kangasluoma, J., Chan, T., Yan, C., Chu, B., Daellenbach, K. R., Bianchi, F., Kokkonen, T. V., Liu, Y., Kujansuu, J., Kerminen, V.-M., Petäjä, T., Wang, L., Jiang, J., and Kulmala, M.: Variation of size-segregated particle number concentrations in wintertime Beijing, *Atmos. Chem. Phys.*, 20, 1201–1216, <https://doi.org/10.5194/acp-20-1201-2020>, 2020.



## Tables

340 Table 1. Statistics of the CIC Channel 1 (small ion) and Channel 2–3 (roughly 2–2.3 nm ion)  
 341 concentrations ( $\text{cm}^{-3}$ ) during 16.01.2024–01.04.2024. Positive polarity is marked by + and  
 342 negative by –. The negative concentrations for the Channel 2 subtracted by Channel 3 are  
 343 indicative of a noisy signal of the instrument.

344  
 345

	Channel 1		Channel 2 - Channel 3	
	+	–	+	–
Mean	280	220	2.8	5.2
10%	130	90	–11	–13
25%	190	140	–4.4	–5.6
50%	270	210	1.3	0.9
75%	360	290	7.9	9.6
90%	430	380	17	24

346  
 347  
 348

349 Table 2. Statistics of NAIS concentrations ( $\text{cm}^{-3}$ ) during 16.01.2024 – 01.04.2024, excluding  
 350 16–17.03.2024. Small ions in the diameter ranges 0.8–2 nm and 1–2 nm are included.  
 351 Intermediate ion concentrations are included for diameter range 2–2.3 nm, as well as for the  
 352 diameter range that the CIC covers (virtual CIC Ch 2–3). Ch 2–3 concentrations have been  
 353 calculated by multiplying the NAIS ion concentrations by detection efficiencies presented in  
 354 Figure 1, after which they have been summed and divided by the average detection  
 355 efficiency. Positive polarity is marked by + and negative by –.

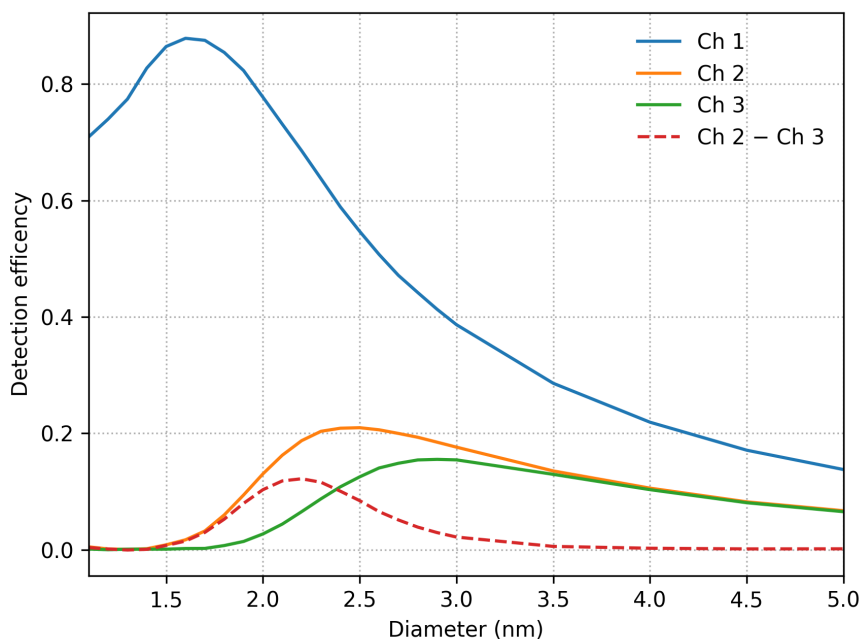
356

	0.8–2 nm		1–2 nm		2–2.3 nm		Virtual CIC channel 2–3	
	+	–	+	–	+	–	+	–
Mean	490	540	400	210	2.0	2.3	17	13
10%	360	400	270	95	0.2	0.04	8.7	2.8
25%	410	460	330	120	0.7	0.3	11	4.5
50%	490	530	400	180	1.5	1.1	14	7.5
75%	570	620	470	270	2.7	2.6	19	14
90%	640	700	540	380	4.2	4.8	29	26

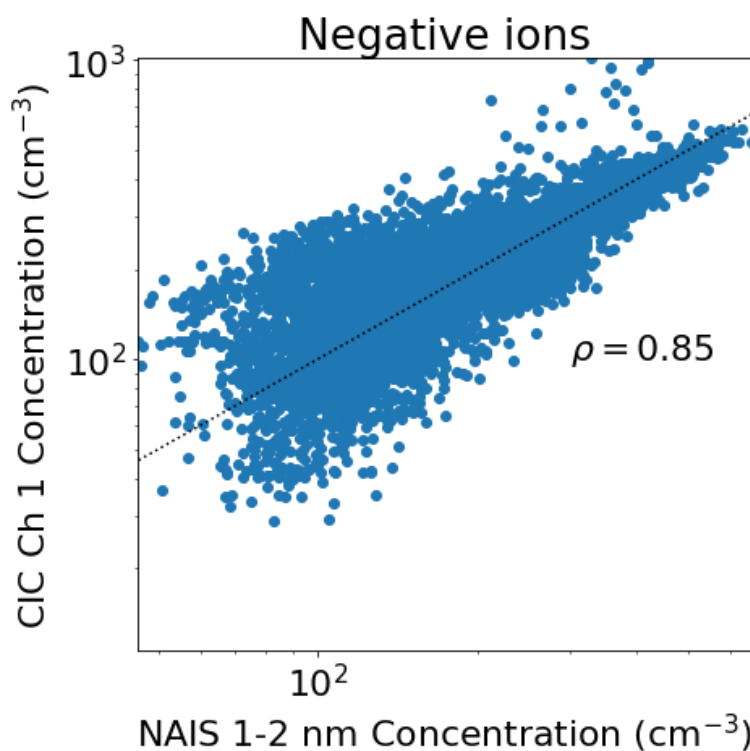
357  
 358  
 359



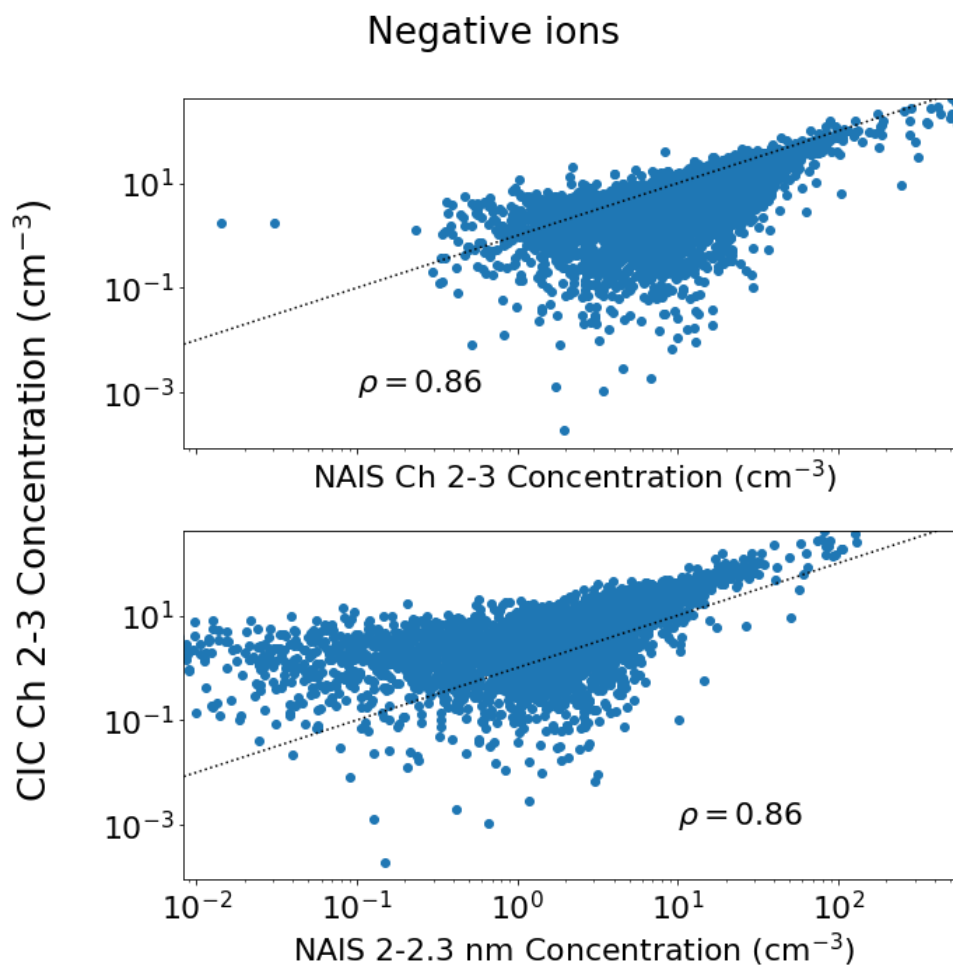
360  
361 **Figures**  
362  
363



364  
365  
366  
367 Figure 1. Experimental detection efficiency for ions in the range from 1.1 to 5.0 nm for each  
368 of the 3 collecting electrodes of the CIC. Due to the absence of a separate sheath air flow  
369 layer in the mobility analyzer, the detection efficiencies do not have a sharp upper size limit;  
370 instead, they asymptotically approach zero as particle size increases. Ion concentrations in a  
371 narrower size range can be estimated by subtracting the signal of channel 3 from channel  
372 2. The detection efficiencies of the two channels converge from 2.5 nm to 3.5 nm and are  
373 practically equal for larger particles.  
374  
375  
376

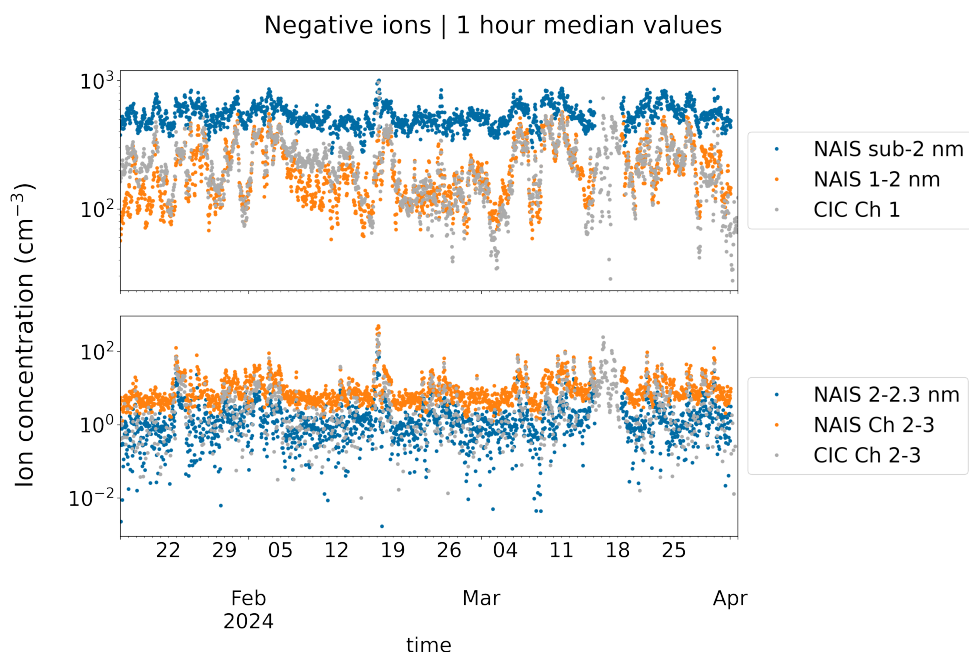


377  
378 Figure 2. Scatter plot of the 15-min median negative small ion concentration measured with  
379 the CIC as a function of the concentration measured with the NAIS in Hyytiälä during 16.01–  
380 01.04. 2024. The values are missing from the period 16–17.03.2024. The NAIS  
381 concentrations are from the diameter range 1–2 nm, while the CIC concentrations are from  
382 Channel 1. The black dotted line marks the 1:1 line. Pearson correlation coefficient  $\rho$  of the  
383 two concentrations shown is included in the figure.  
384  
385



386  
387  
388  
389  
390  
391  
392  
393  
394  
395  
396  
397  
398  
399  
400  
401  
402  
403

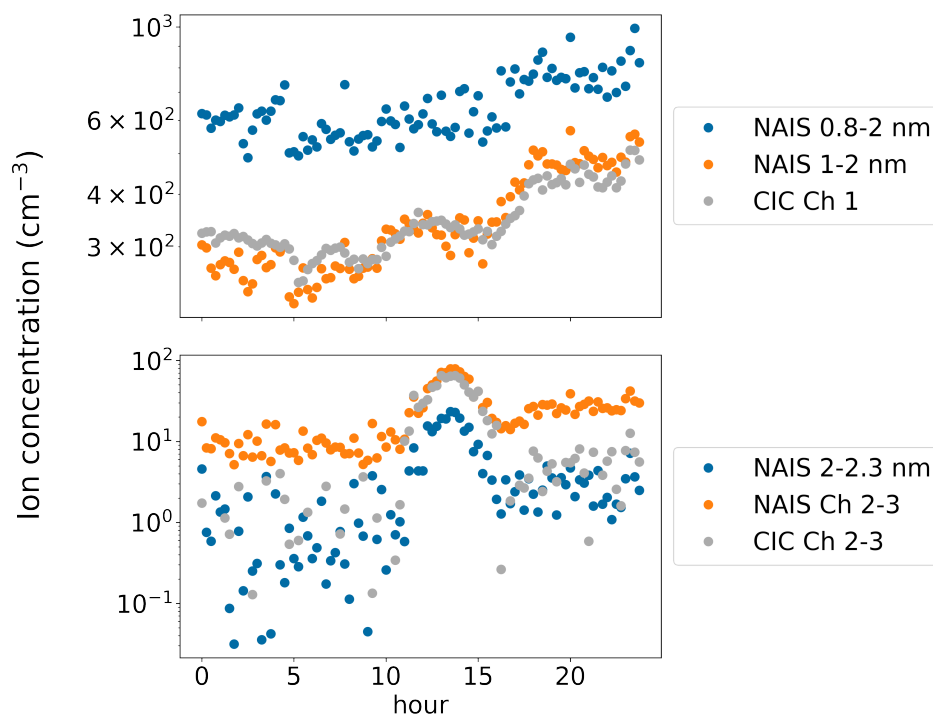
Figure 3. Scatter plot of approximately 2.0–2.3 nm negative ion 15-minute-median concentrations measured with the CIC as a function of concentrations measured with the NAIS in Hyytiälä during 16.01–01.04. 2024. The values are missing from the period 16–17.03.2024. The NAIS concentrations on the top figure were determined for the same size range as covered by the CIC Channels 2 and 3. The concentrations from the NAIS were multiplied by the detection efficiencies for the CIC Channel 2–3 presented in Figure 1, summed and divided by the average detection efficiency for the CIC channel 2–3. If the NAIS concentrations are assumed to be equal to the atmospheric concentrations, then in theory the CIC and NAIS concentrations in the top figure should be equal. The NAIS concentrations on the bottom figure are for the diameter range 2–2.3 nm. The black dotted line marks the 1:1 line. Pearson correlation coefficient  $\rho$  of the two concentrations shown is included in the figure. The NAIS concentrations in the top figure are on average higher, which is due to the wider size range of ions covered.



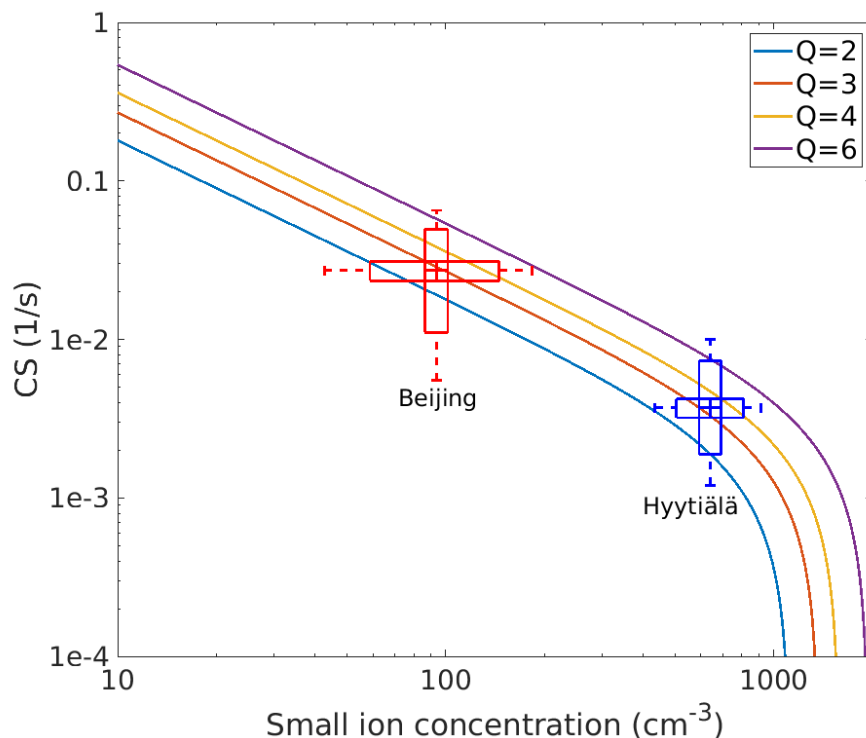
404  
405 Figure 4. Time series of observed ion concentrations (16.01.2024–01.04.2024). The NAIS  
406 data are missing from the period 16–17.03.2024. The top figure has the concentrations of  
407 small ions from the CIC Channel 1 and from the NAIS for both all sub-2 nm ions and 1–2 nm  
408 ions. The bottom figure has concentrations of ions measured by the CIC channel 2–3 which  
409 approximately corresponds to the size range of 2–2.3 nm. In addition, there are  
410 concentrations of 2–2.3 nm ions measured by the NAIS (NAIS 2–2.3 nm) and concentrations  
411 from the NAIS that were derived by multiplying the NAIS concentrations by the CIC  
412 detection efficiencies presented in Figure 1 and then summed and divided by the average CIC  
413 concentrations (NAIS Ch 2-3). In theory, if the concentrations measured by NAIS are  
414 assumed to equal to the atmospheric ion concentrations, then the CIC Ch 2–3 and NAIS Ch  
415 2–3 concentrations should be equal.  
416



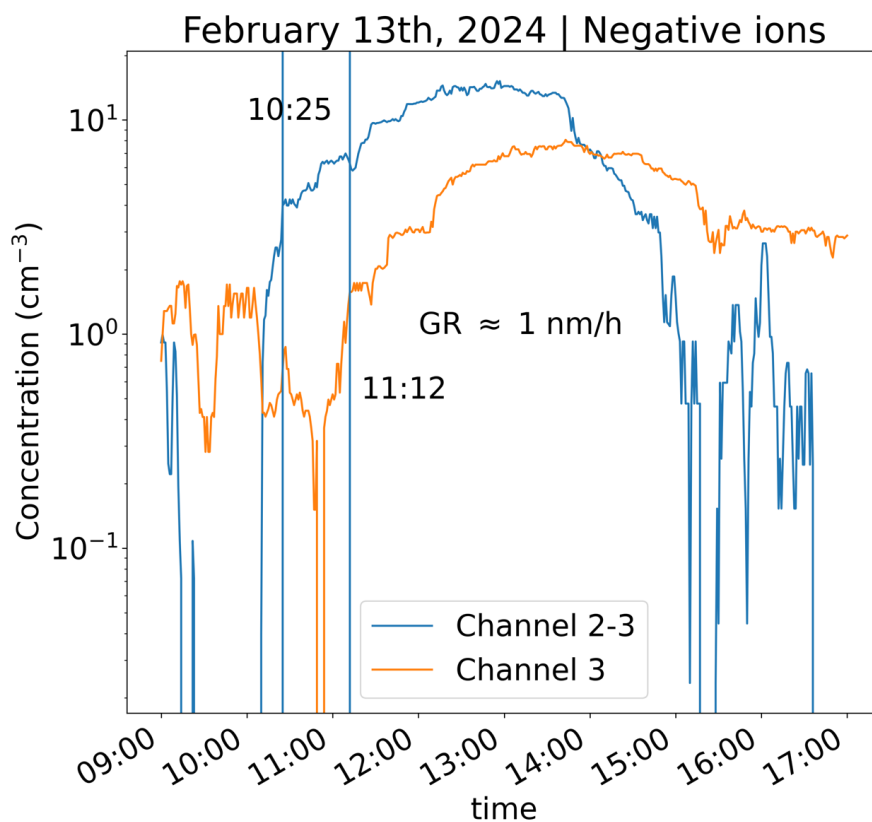
### Negative ions | 2024-03-10 | 15 min median values



417  
418 Figure 5. Observed negative ion concentrations on 10.03.2024. The top figure has the  
419 concentrations of small ions. For CIC, they are from the CIC Channel 1. From the NAIS,  
420 concentrations for all sub-2 nm ions and based on the size range 1–2 nm are included. The  
421 top figure illustrates how the CIC concentrations correspond closely to the concentrations  
422 of 1–2 nm ions, while ions smaller than are not detected. The bottom figure has the  
423 concentrations of intermediate ions. For CIC, they are from Channel 2–3, corresponding to  
424 roughly 2–2.3 nm size range. For NAIS, the concentrations of ions between 2 and 2.3 nm are  
425 included, as well as the concentrations derived by multiplying the NAIS concentrations by  
426 the CIC detection efficiencies presented in Figure 1 and then summed and divided by the  
427 average CIC concentrations (NAIS Ch 2–3). In theory, if the concentrations measured by the  
428 NAIS are assumed to equal the atmospheric ion concentrations, then the CIC Ch 2–3 and  
429 NAIS Ch 2–3 concentrations should be equal. When the concentrations are higher around  
430 midday, this is indeed the case. The correlation coefficients on this day are 0.83, 0.95, 0.93  
431 and 0.90 for NAIS 0.8–2 nm vs CIC Channel 1, NAIS 1–2 nm vs CIC Channel 1, NAIS 2–2.3  
432 vs CIC Channel 2–3, and NAIS Channel 2–3 vs CIC Channel 2–3, respectively.  
433  
434



435  
436 Figure 6. Condensation sink (CS) as function of the small ion concentration for different ion  
437 source rates ( $Q$ , ions  $\text{cm}^{-3} \text{s}^{-1}$ ). The observed values of  $N$  and CS in Hyytiälä and Beijing  
438 (medians marked by the center line of the boxplot, 25% and 75% quartiles marked by the  
439 edges, and 10% and 90% percentiles marked by the whiskers of the boxplots) indicate ion  
440 source rates between about 2 and 4  $\text{cm}^{-3} \text{s}^{-1}$  in both places. For Hyytiälä, the data covers most  
441 of time from the beginning of 2016 to the end of 2020. For Beijing, the ion concentrations are  
442 determined based on the values from 13.01.2018 to 01.04.2020, whereas the CS data cover  
443 the period 20.02.2018 to 31.03.2019.  
444  
445  
446  
447



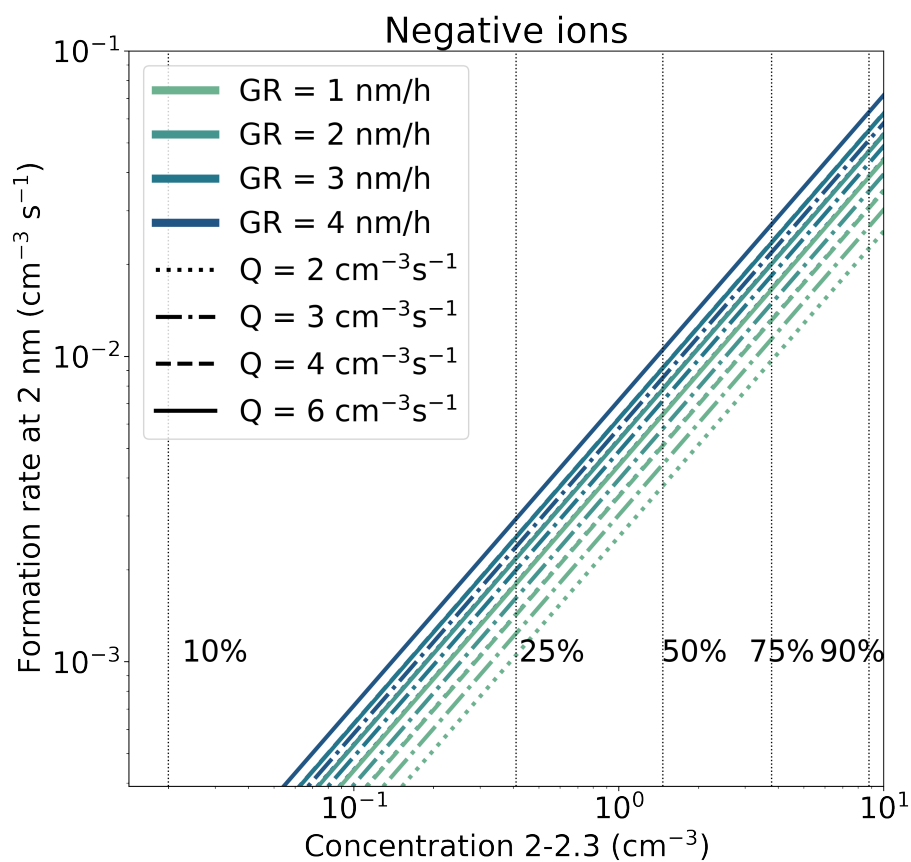
448

449

450 Figure 7: Determining an approximation for ion growth rate (GR). The ion concentrations  
451 were smoothed using a moving 1-hour median method to lessen the impact of noise. Channel  
452 3 and Channel 2–Channel 3 concentrations have a similar shape between 10:00 and 16:00,  
453 and the shape of the Channel 3 roughly follows that of Channel 2–3 with a time delay.  
454 Considering the shape and features of the two curves, and the times at which the two  
455 concentrations reach a similar fraction of the maximum concentration (similar to appearance  
456 time method), two time instances were identified visually. The ion concentrations are around  
457 0.2 of the corresponding maximum concentrations at these times. From these approximate  
458 appearance times, a time delay is gained and assuming the diameters of 2.1 nm and 2.9 nm  
459 for Channel 2–3 and 3, respectively, we obtain a GR of about 1.0 nm/h. We note that on this  
460 particular example day, the curves follow each other closely for a span of several hours, so  
461 that the value of GR is not very sensitive to the identified appearance times, i.e., the chosen  
462 fraction of the maximum concentration anywhere between 0.2 and 0.9 results in the same  
463 approximate GR  $\approx$  1 nm/h. However, if the two concentration curves are not as similar, and  
464 if there is variation in the features, more care in identifying the appearance times may be  
465 needed.

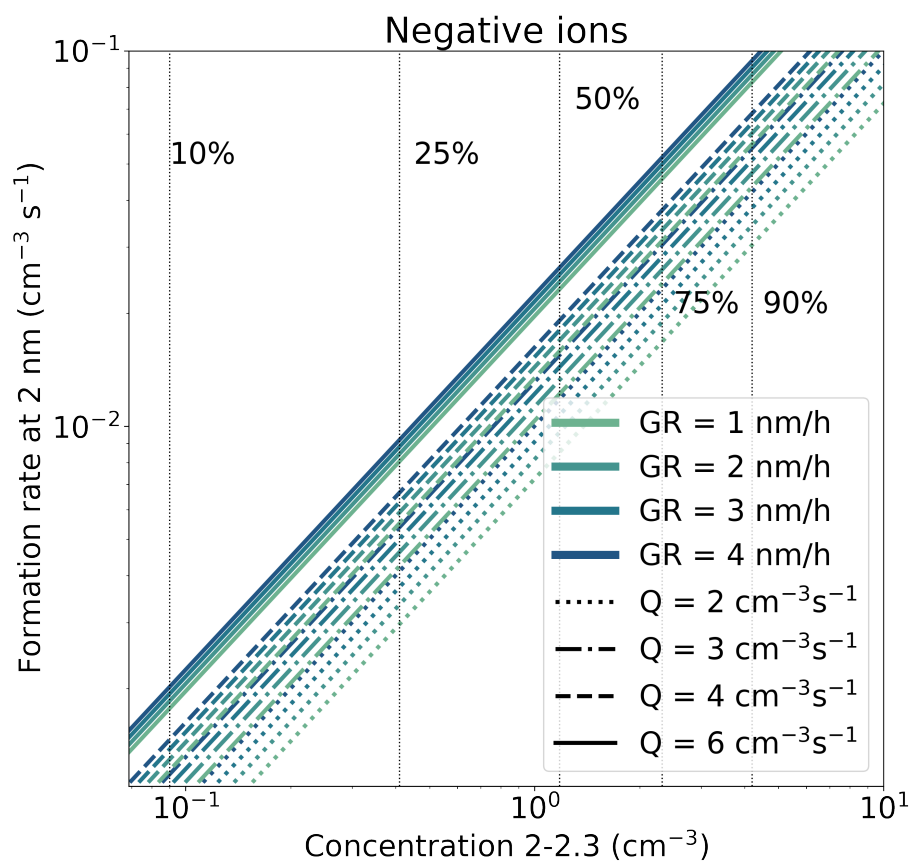


466  
467



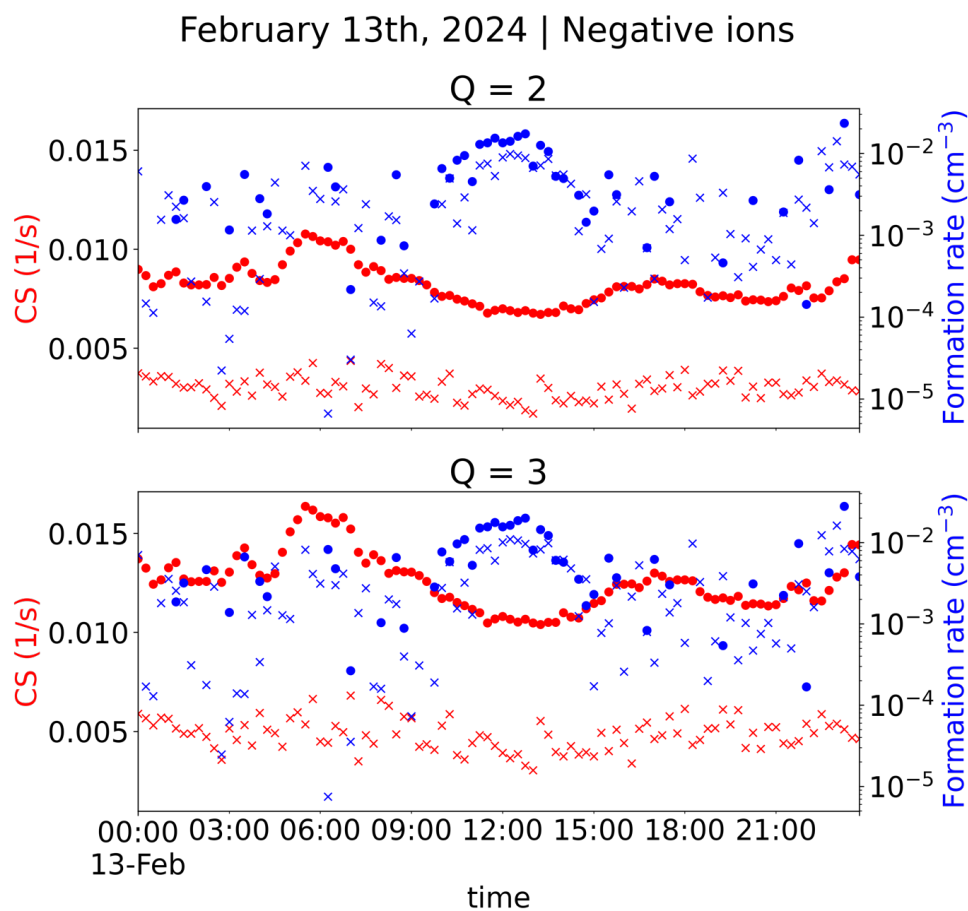
468  
469 Figure 8. The estimated formation rate of 2-nm ions (negative ions). The formation rate using  
470 the GR of 1 nm/h can be estimated as a function of concentration of 2.0–2.3 nm size ions in  
471 Hyytiälä. The 10%, 25%, 50% (median), 75%, and 90% concentration values from Hyytiälä  
472 are indicated by the vertical dotted lines.

473  
474  
475



476  
477 Figure 9. The estimated formation rate of 2 nm ions (negative ions). The formation rate using  
478 the GR of 1 nm/h can be estimated as a function of concentration of 2.0-2.3 nm size ions in  
479 Beijing. The 10%, 25%, 50% (median), 75%, and 90% concentration values from Beijing are  
480 indicated by the vertical dotted lines.

481  
482  
483  
484  
485  
486  
487



488  
489  
490  
491  
492  
493  
494  
495  
496  
497

Figure 10: Condensation sink (right) and formation rate of 2 nm ions (left). The values marked by dots are based on CIC channel 1 and channel 2-3 ion negative ion concentrations while the values marked by x markers are based on NAIS sub-2 nm and 2-2.3 nm negative ion concentrations. The top panel has valued with assumed ion source rate of  $Q = 2 \text{ cm}^{-3} \text{ s}^{-1}$  while the bottom panel includes those for  $Q = 3 \text{ cm}^{-3} \text{ s}^{-1}$ . A value of 1 nm/h for GR used, as determined in Fig. 7 for this day. Negative and positive ion concentrations were assumed to be the same.